PCCP

PAPER

View Article Online
View Journal

Cite this: DOI: 10.1039/c6cp00053c

Atmospheric fates of Criegee intermediates in the ozonolysis of isoprene†

Tran B. Nguyen,‡*[a] Geoffrey S. Tyndall,[b] John D. Crounse,[a] Alexander P. Teng,[a] Kelvin H. Bates,[c] Rebecca H. Schwantes,[a] Matthew M. Coggon,§[c] Li Zhang,[d] Philip Feiner,[d] David O. Milller,[d] Kate M. Skog,[e] Jean C. Rivera-Rios,¶[e] Matthew Dorris,[e] Kevin F. Olson,‖[fg] Abigail Koss,[h] Robert J. Wild,[hi] Steven S. Brown,[h] Allen H. Goldstein,[fg] Joost A. de Gouw,[h] William H. Brune,[d] Frank N. Keutsch,¶[e] John H. Seinfeld[cj] and Paul O. Wennberg[aj]

We use a large laboratory, modeling, and field dataset to investigate the isoprene + O_3 reaction, with the goal of better understanding the fates of the C_1 and C_4 Criegee intermediates in the atmosphere. Although ozonolysis can produce several distinct Criegee intermediates, the C_1 stabilized Criegee (CH_2OO, 61 ± 9%) is the only one observed to react bimolecularly. We suggest that the C_4 Criegees have a low stabilization fraction and propose pathways for their decomposition. Both prompt and non-prompt reactions are important in the production of OH (28% ± 5%) and formaldehyde (81% ± 16%). The yields of unimolecular products (OH, formaldehyde, methacrolein (42 ± 6%) and methyl vinyl ketone (18 ± 6%)) are fairly insensitive to water, *i.e.*, changes in yields in response to water vapor (≤4% absolute) are within the error of the analysis. We propose a comprehensive reaction mechanism that can be incorporated into atmospheric models, which reproduces laboratory data over a wide range of relative humidities. The mechanism proposes that $CH_2OO + H_2O$ ($k_{(H_2O)} \sim 1 \times 10^{-15}$ cm^3 molec^{-1} s^{-1}) yields 73% hydroxymethyl hydroperoxide (HMHP), 6% formaldehyde + H_2O_2, and 21% formic acid + H_2O; and $CH_2OO + (H_2O)_2$ ($k_{(H_2O)_2} \sim 1 \times 10^{-12}$ cm^3 molec^{-1} s^{-1}) yields 40% HMHP, 6% formaldehyde + H_2O_2, and 54% formic acid + H_2O. Competitive rate determinations ($k_{SO_2}/k_{(H_2O)n=1,2} \sim 2.2$ (±0.3) × 10^4) and field observations suggest that water vapor is a sink for greater than 98% of CH_2OO in a Southeastern US forest, even during pollution episodes ([SO_2] ~ 10 ppb). The importance of the $CH_2OO + (H_2O)_n$ reaction is demonstrated by high HMHP mixing ratios observed over the forest canopy. We find that CH_2OO does not substantially affect the lifetime of SO_2 or HCOOH in the Southeast US, *e.g.*, $CH_2OO + SO_2$ reaction is a minor contribution (<6%) to sulfate formation. Extrapolating, these results imply that sulfate production by stabilized Criegees is likely unimportant in regions dominated by the reactivity of ozone with isoprene. In contrast, hydroperoxide, organic acid, and formaldehyde formation from isoprene ozonolysis in those areas may be significant.

Received 4th January 2016,
Accepted 16th March 2016

DOI: 10.1039/c6cp00053c

www.rsc.org/pccp

[a] Division of Geological and Planetary Sciences, California Institute of Technology, Pasadena, California, USA. E-mail: tbn@ucdavis.edu
[b] Atmospheric Chemistry Observations & Modeling Laboratory, National Center for Atmospheric Research, Boulder, CO, USA
[c] Division of Chemistry and Chemical Engineering, California Institute of Technology, Pasadena, California, USA
[d] Department of Meteorology, The Pennsylvania State University, University Park, PA, USA
[e] Department of Chemistry, University of Wisconsin at Madison, Madison, WI, USA
[f] Department of Environmental Science, Policy, and Management, University of California at Berkeley, Berkeley, CA, USA
[g] Department of Civil and Environmental Engineering, University of California at Berkeley, Berkeley, CA, USA
[h] Earth Systems Research Laboratory, Chemical Sciences Division, National Oceanographic and Atmospheric Administration, Boulder, CO, USA
[i] Cooperative Institute for Research in Environmental Sciences, University of Colorado, Boulder, CO, USA
[j] Division of Engineering and Applied Science, California Institute of Technology, Pasadena, California, USA

† Electronic supplementary information (ESI) available. See DOI: 10.1039/c6cp00053c

‡ Now at Department of Environmental Toxicology, University of California, Davis, Davis, CA, USA.
§ Now at Earth Systems Research Laboratory, Chemical Sciences Division, National Oceanographic and Atmospheric Association, Boulder, CO, USA.
¶ Now at Department of Chemistry and Chemical Biology, Harvard University, Cambridge, MA, USA.
‖ Now at Chevron Corp, San Ramon, CA, USA.

1. Introduction

Ozonolysis is one of the main atmospheric oxidation pathways for volatile alkenes. Reaction with ozone globally removes ~10% of isoprene (C_5H_8), the most abundant alkene in the atmosphere. For monoterpenes ($C_{10}H_{16}$) and sesquiterpenes ($C_{15}H_{24}$), ozonolysis is a substantially larger sink due to their faster rate coefficients with ozone.[1] The first steps of the alkene ozonolysis mechanism are shown in Fig. 1.[2] Two primary ozonides (POZ) are formed from ozone addition at either double bond of isoprene, decomposing into methacrolein (MACR), methyl vinyl ketone (MVK), formaldehyde (HCHO), and potentially up to nine activated Criegee intermediates (CI, denoted with asterisk). The C_4 Criegees (MACR-OO* and MVK-OO*) can be formed with four conformations each that are *syn* or *anti* to methyl or vinyl groups. The CI can experience a few unimolecular processes – most notably, decomposition[3] into a hydroxyl radical (OH) and a beta-oxy alkyl radical (R) and thermalization by atmospheric gases to form the stabilized Criegee intermediate (SCI). In addition, a fraction of SCI has been suggested to be formed through POZ decomposition.[4] Most of the OH from isoprene ozonolysis is thought to be produced by the *syn*-methyl MVK-OO conformers (Fig. 1, g and h) *via* the formation of a vinyl hydroperoxide (VHP) intermediate.[5–9]

The stabilized Criegees (SCIs) may undergo bimolecular reaction with a number of atmospheric species, including water vapor (H_2O), sulfur dioxide (SO_2), formic acid (HCOOH), carbonyls (*e.g.*, HCHO and acetaldehyde), NO, NO_2, O_3, RO_2, alkenes, among others.[10–16] Even if a substantial fraction of CIs are stabilized, they may still experience unimolecular losses. The structure, and even conformation, of the SCI dictate their unimolecular and bimolecular reactivities,[9] with *syn* SCI more susceptible to decomposition. The simplest SCI (CH_2OO) has special importance in atmospheric chemistry as it is produced by all exocyclic alkenes, including isoprene. Unlike other SCIs, however, CH_2OO is non-*syn* (*i.e.*, not facing any hydrocarbon groups), which greatly reduces its unimolecular reactivity.[17]

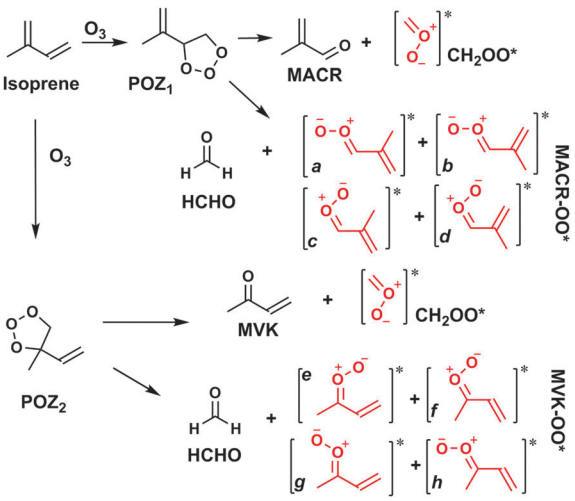

Fig. 1 The first steps of the Criegee mechanism of ozonolysis, shown for isoprene. Criegee intermediates are drawn as zwitterions; however, depending on the chemical structure, they may also have diradical character.

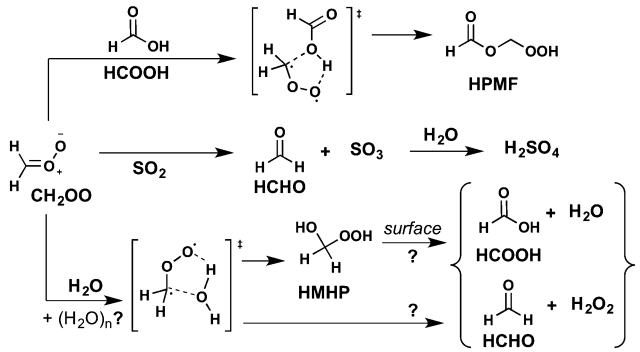

Fig. 2 The reaction of CH_2OO with HCOOH, SO_2, and H_2O (and possibly water clusters). The production of HCOOH + H_2O and HCHO + H_2O_2 from the water reaction has been suggested to (at least partially) result from surface-mediated decomposition of HMHP;[27] however, it is not clear if there are direct routes to these products from CH_2OO + H_2O.

Fig. 2 shows a simplified reaction scheme between CH_2OO and water (or water clusters),[18–21] sulfur dioxide (SO_2), and formic acid (HCOOH). The CH_2OO + $(H_2O)_n$ reaction (where n = 1, 2, ...) produces hydroxymethyl hydroperoxide (HMHP), hydrogen peroxide (H_2O_2) + formaldehyde (HCHO), and formic acid (HCOOH) + H_2O as main products.[22–28] The CH_2OO + HCOOH reaction produces hydroperoxy methylformate (HPMF).[23,27,29] Finally, the CH_2OO + SO_2 reaction produces SO_3, which then reacts with water to form H_2SO_4.[30]

Certain populations of SCIs may produce OH,[31] perhaps analogously to the hot Criegee VHP channel, among other products. Decomposition of SCIs is rarely discussed within the scope of the atmospheric fates; however, it is an important consideration in understanding their total reactivity. Previously published unimolecular decomposition rates for larger Criegees have high uncertainty, so the following is only a qualitative discussion. SCI decomposition rates has been shown to increase with size.[11,32] For example, even though the thermalized acetone oxide ($(CH_3)_2COO$) has been recently reported to undergo a diffusion-limited reaction with SO_2,[33] its short unimolecular lifetime due to its all-*syn* conformation, *i.e.*, both sides facing methyl groups, severely limits the atmospheric relevance of its bimolecular reactions (τ_{uni} = 0.001–0.004 s).[32–34] It should be noted that experimental determinations of unimolecular lifetimes (*e.g.*, 0.002 s)[33] may have some contribution from Criegee self-reaction; thus, τ_{uni} may be closer to the higher end of the reported range. The ratio k_{decomp}/k_{SO_2} for *syn*-CH_3CHOO and $(CH_3)_2COO$ have been measured to be 1 and 2 orders of magnitude higher than that for CH_2OO, respectively.[32] Thus, even in a polluted atmosphere (~10 ppb SO_2 and 50% RH at room temperature), decomposition using the Olzmann *et al.* (1997) lower-limit rate coefficient accounts for the majority (~76%) of the acetone oxide fate, while the reaction with SO_2 is minor (~8%). The Newland *et al.* (2015) relative rate coefficient (using k_{SO_2} of Huang *et al.* (2015)) predicts an even higher decomposition fraction.

The present work focuses on understanding the bimolecular reactive channels of CH_2OO and, more generally, the mechanism of isoprene ozonolysis in the atmosphere. We neglect the unimolecular reactions for CH_2OO, as it has a long lifetime with respect to decomposition at 298 K and 1 atm ($\sim$3 s).[34] Furthermore, we provide suggestions for a unifying reaction scheme that may be incorporated into atmospheric models.

2. Experimental

2.1. Chamber methods

Experiments were conducted in the Caltech dual 24 m^3 Teflon environmental chambers at $\sim$295 K and $\sim$1 atm. A subset of the work was performed as part of the FIXCIT campaign and the overview manuscript[35] provides an in-depth description of the chamber and relevant experiments. Product yield studies were investigated with isoprene and ozone mixing ratios of $\sim$100 and 600 ppb, respectively, and relative humidity (RH) in the approximate range of $<$4–76%. The production of OH was investigated in the absence of a chemical scavenger, but all other studies were performed with excess cyclohexane (50 ppm) to scavenge OH. Although excess cyclohexane is used, a minor fraction of the products will result from OH chemistry. Relative rate experiments were used to investigate the competition between SO_2 and H_2O at lower isoprene and ozone mixing ratios ($\sim$25 ppb and 100 ppb, respectively) and 10 ppm cyclohexane.

RH inside the reaction chambers was adjusted to the desired level at the beginning of each experiment with a Nafion membrane humidifier (Permapure, LLC) and recirculating ultra-purified water (Millipore Milli-Q, 18 MΩ, $<$3 ppb TOC). The RH was stable throughout each experiment, as verified by a Vaisala HMT221 probe that was calibrated in the range of 11–95% with saturated salt solutions. Water vapor in the range of RH $<$ 10% was measured by chemical ionization mass spectrometry (CIMS, see Section 2.2). However, the accuracy of RH measurements degrades in the lower range due to the difficulty in determining small mixing ratios of H_2O; thus we quote "dry" RH as "$<$4%". Although RH in dry conditions is quoted as an upper bound, we estimate the actual RH in the chamber is closer to 1%. Ozone was introduced into the chamber by flowing air through a commercial UV ozone generator. Reagents, *e.g.*, isoprene (Aldrich, $\geq$99%) cyclohexane (CHX, Aldrich $>$99%), were introduced into the chamber by volumetric injection of liquid material using Hamilton gas-tight syringes. In general, the order of introduction was water vapor, ozone, cyclohexane, and then isoprene. For relative rate studies, gaseous SO_2 (standard mixture 10 ppm in N_2, Scott Specialty Gases) was introduced into the chamber using a calibrated mass flow controller. After injection of isoprene, several short high-pressure pulses of air were introduced into the chamber to homogenize the contents of the chamber so that the reaction can start immediately and uniformly. We verified that injected gases were well-mixed in $<$5 minutes using this method. The duration of a typical experiment was 5–7 hours.

2.2. Analytical quantification

Isoprene, methacrolein (MACR), methyl vinyl ketone (MVK), and cyclohexane (CHX) were quantified by gas chromatography with a flame ionization detector (GC-FID). The GC-FID was calibrated with commercial standards (Aldrich) in the range of 20–200 ppb by use of volumetric gas-tight syringes and a calibrated mass flow of N_2 into a 100L Teflon calibration bag. Additionally, the absolute quantities of ISOP, MACR, and MVK was cross calibrated using Fourier transform infrared spectroscopy (FT-IR) in the range of 1–20 ppm *via* a similar method. The ppm-level calibration bags were quantified with FT-IR using tabulated absorption cross sections[36] before sampling with GC-FID. The mixing ratio of ozone was quantified by a calibrated ozone absorption monitor (Horiba APOA-360). The mixing ratios of NO and NO_2 were quantified with a commercial NO_x monitor (Teledyne T200). NO was observed at baseline level (limit of detection 0.5 ppb) and NO_2 remained below 5 ppb during ozonolysis experiments. Sulfuric acid aerosols were measured using a time-of-flight aerosol mass spectrometer (AMS, Aerodyne)[37] and data processing was performed using the Pika 1.14D analysis module in Igor Pro. The instrumental ionization efficiency was calibrated with 350 nm ammonium nitrate particles.

Formaldehyde and HO_x (OH and HO_2) were measured *in situ* by two laser-induced fluorescence (LIF) instruments during the FIXCIT campaign. The University of Wisconsin (UW) LIF instrument[38,39] quantified formaldehyde from the difference between its online (353 nm) and offline signal. The Pennsylvania State University (PSU) Ground-based Tropospheric Hydrogen Oxides Sensor (GTHOS)[40] measured OH and HO_2 by the fluorescent assay by gas expansion (FAGE) technique. OH was quantified spectroscopically (near 308 nm) and the zero background is determined using hexafluoropropene (C_3F_6) as an OH scrubber in the instrument inlet. HO_2 was measured after its chemical conversion in the instrument inlet to OH using pure NO (HO_2 + NO $\rightarrow$ OH + NO_2). The known interference of HO_2 measurement by RO_2 radicals[41] was corrected in the following manner: the NO addition to GTHOS was modified to reduce the reaction time and the amount of NO added. Although the conversion of HO_2 to OH was decreased from $\sim$90% to less than 10%, the conversion of RO_2 to OH was reduced to less than 1%, so that more than 95% of the signal was due to converted HO_2 and only a few percent was due to RO_2.[41] These conversion rates were measured with GTHOS in the Brune laboratory at PSU and are similar to those determined by Fuchs *et al.* (2011).

Gas-phase hydroperoxides (H_2O_2, HMHP, MHP, *etc.*), acidic compounds (SO_2, HCOOH, *etc.*), and other volatiles with more than one polar functional group (*e.g.*, hydroxy carbonyls) are quantified with a triple-quadrupole chemical ionization mass spectrometer (CIMS) using CF_3O^- as an ionization reagent.[42,43] The sample flow from the chamber was diluted by a factor of 12 with dry N_2 before mass spectrometry analysis. The dry (RH $<$ 4%) sensitivity of triple-quadrupole CF_3O^- CIMS to different analytes was cross-calibrated with a CF_3O^- time-of-flight (ToF) CIMS during the FIXCIT campaign. The ToF CIMS was calibrated for a variety of compounds (H_2O_2, HMHP, HCOOH, SO_2, peracetic acid (PAA), acetic acid (AA), hydroxyacetone (HAC), *etc.*)

with commercial or synthesized standards based on gravimetric or spectrometric techniques (see Section S3 of ref. 44 for more information). Table S1 (ESI†) provides more information about CIMS detection of the major compounds discussed in this work. The CIMS measurement uncertainties are approximately 20–30% for calibrated compounds (*e.g.*, HCOOH) and ~50% for uncalibrated compounds (*e.g.*, HPMF).

In addition to the dry sensitivity, the dependence of the ion chemistry on water vapor is unique to each CIMS instrument and is critical for the accurate interpretation of RH-dependent yields. We obtained the water-dependent calibration curves in the experimental RH range by introducing a sample stream (containing a stable gaseous source of each compound) and a dilution stream that has tunable water vapor content to the CIMS flow tube region. The water vapor mixing ratio of the dilution stream was achieved by mixing flow-controlled quantities of a humid air stream ([H_2O] ~ 3%, quantified by FT-IR) and a dry N_2 stream ([H_2O] < 100 ppm). A stable source of HMHP, for which a commercial standard is unavailable, was synthesized in the Teflon chamber using the HCHO + HO_2 reaction,[45] which produces a low yield of HMHP. The photolysis of HCHO (~2 ppm) generates the HO_2 that is needed to react with HCHO. The UV lights were turned off after approximately 1 hour, and the ~6 ppb HMHP formed during the photolytic period was stable in the dark indefinitely. A typical water-dependent calibration alternates a dry data point with several humid points and zeros (where sample flow is shut off), after each period is allowed to stabilize (Fig. S1, ESI†). Water curves were obtained for HCOOH, H_2O_2, and SO_2 using commercial standards as the sample source, in an identical manner. The sensitivity of the CIMS toward HPMF was not measured, but was assumed to be similar to HMHP based on the molecular characteristics of these two compounds.[46]

2.3. Wall loss corrections

Alpha-hydroxy hydroperoxides like HMHP have a propensity to participate in heterogeneous reactions on humid surfaces.[27] Thus, we measured wall loss rates for HMHP, HCOOH, and H_2O_2 as a function of RH to correct for this effect. HMHP was synthesized *via* an alternative method to the one described in Section 2.2: a gaseous mixture of formaldehyde/N_2 (produced by flowing dry N_2 past heated paraformaldehyde solid) was bubbled into an aqueous H_2O_2 solution (50% v/v). The outflow of the bubbler (containing HCHO, HMHP, HCOOH, and H_2O_2) was introduced into the chamber until the signal of HMHP in CIMS was adequate, after which the flow was stopped and the wall loss was monitored for 8–10 hours. The production of HCOOH from HMHP conversion may obscure the HCOOH wall loss to a degree. However, by virtue of the synthesis method (high water content in the H_2O_2 bubbler), the HCOOH mixing ratio in the chamber was more abundant than HMHP by a factor of 100, so that even if all of the HMHP were converted to HCOOH, the production yield signal would impact k_{wall} of HCOOH by only 1%. We did not observe noticeable wall loss of HMHP, HCOOH, or H_2O_2 under dry conditions (Fig. S2, ESI†); however, the wall loss rates become non-negligible at the highest RH investigated (72%), where HMHP was removed at a rate of approximately 0.1% per minute. The humidity-dependent wall loss rates ($k_{wall\_HMHP} = -1.4 \times 10^{-5} \times$ RH min^{-1}, $k_{wall\_H_2O_2} = -9.6 \times 10^{-6} \times$ RH min^{-1}, and $k_{wall\_HCOOH} = -2.2 \times 10^{-6} \times$ RH min^{-1}) were used to correct the CIMS data.

3. Results and discussion

3.1. Humidity-dependent product yields

The molar yields of products from the isoprene ozonolysis in the RH range of <4–76% are reported in Table 1. Fig. 3 shows

Table 1 Molar yields of major products for different RH and SO_2 conditions. Initial conditions of ISO and O_3 in B are similar to A, except CHX was not added as a reagent. CH_2OO yields for A are obtained by summing the yields of CH_2OO + $(H_2O)_n$ and CH_2OO + HCOOH products measured using CIMS. In C, CH_2OO yield determinations include the measurement of H_2SO_4 aerosol using AMS. See Table S2 (ESI) for details on quantification with CIMS. Missing entries indicate unavailability of instruments or irrelevancy of data. Measurement uncertainties are: SO_2 (±20%), CH_2OO (±15 AMS, ±30% CIMS), MACR (±15%), MVK (±33%), OH (±25%), HCHO (±20%), HCOOH (±10%), H_2O_2 (±20%), HMHP (±20%), HPMF (±50%). BDL = below detection limit for GC-FID

Experiment type (T = 295 K)	SO_2 (ppb)	RH (%)	Yield (CH_2OO)	Yield (MACR)	Yield (MVK)	Yield (OH)	Yield (HCHO)	Yield (HCO_2H)	Yield (H_2O_2)	Yield (HMHP)	Yield (HPMF)
(A) Product yields	0	<4	0.30	0.39	0.15	—	0.79	0.05	0.012	0.17	0.064
(scavenger)	0	6	0.40	0.39	0.14	—	—	0.07	0.014	0.26	0.060
[ISO] ~ 100 ppb	0	13	0.51	0.41	0.17	—	—	0.09	0.019	0.38	0.030
[O_3] ~ 600 ppb	0	27	0.61	0.41	0.16	—	—	0.13	0.038	0.44	0.013
[CHX] ~ 50 ppm	0	37	0.61	0.41	0.18	—	0.83	0.13	0.044	0.44	0.001
	0	44	0.62	0.42	0.16	—	—	0.15	0.046	0.41	0.005
	0	51	0.61	0.40	0.21	—	—	0.20	0.054	0.34	0.004
	0	73	0.62	0.44	0.19	—	—	0.28	0.066	0.24	0.002
	0	76	0.60	0.41	0.19	—	—	0.28	0.065	0.22	0.003
(B) Product yields	0	4	—	—	—	0.28	—	—	—	—	—
(no scavenger)	0	52	—	—	—	0.28	—	—	—	—	—
(C) Relative rate	15	20	0.60	BDL	BDL	—	—	—	—	—	—
[ISO] ~ 25 ppb	15	3	0.65	BDL	BDL	—	—	—	—	—	—
[O_3] ~ 120 ppb	75	3	0.66	BDL	BDL	—	—	—	—	—	—
[CHX] ~ 10 ppm											

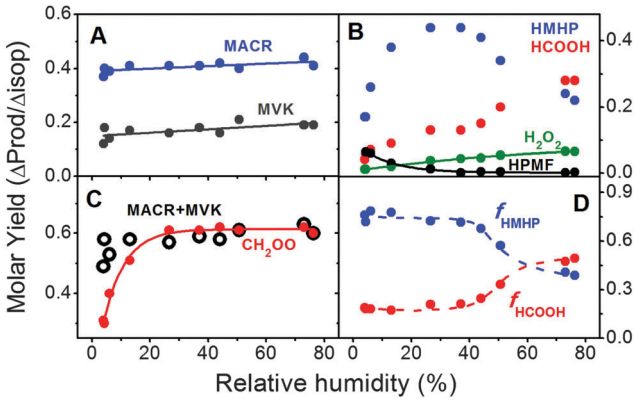

Fig. 3 Molar yields of the isoprene + O_3 reaction products (A–C) at several RH conditions. The CH_2OO yield in panel C is inferred from the sum of the scavenged products of CH_2OO with water vapor and formic acid. Panel D shows the fraction of water-scavenged CH_2OO that is observed as HMHP (f_{HMHP}) and HCOOH (f_{HCOOH}). Solid lines indicate least-squares fits, when applicable, and dashed lines only serve to guide the eyes. HMHP and HCOOH in panel B can each be fit by two exponential curves delineated at RH ~ 40%, but no singular relationship.

the trends in yields of select gas-phase organic products measured by GC-FID and CIMS. As expected, the "prompt" products, *i.e.*, those formed primarily from the decomposition of primary ozonides (POZ) such as HCHO, MACR, and MVK, do not exhibit a strong dependence on water vapor (Fig. 3A and Table 1). This is also true for yields of OH radicals, which are produced from decomposition channels. The observation that OH yields from isoprene ozonolysis are independent of humidity has been reported in other works.[5,47] Further insights on the sources of OH and HCHO yields are obtained by model simulations (see Section 3.2). The yields of carbonyls and OH from this work are not significantly different from those reported elsewhere.[8,9,48–51] The trends in yields for carbonyls are slightly positive with humidity, possibly supporting a minor production from SCI + $(H_2O)_n$ reaction (H_2O_2 as coproduct). However, the measurement uncertainties are significant (10–30%) and, thus, this channel was treated as minor in the development of our mechanism.

Stabilized CH_2OO yields obtained by a chemical scavenging method were similar whether H_2O or SO_2 was used as the Criegee scavenger (Table 1, Y_{SCI} ~ 0.60 using CIMS, and ~0.64 using AMS). As the detection of scavenged products utilized two independently-calibrated instruments, their agreement lends further confidence to the yield results. Our CH_2OO determination is consistent, within uncertainties, with those reported recently (0.56–0.60).[32,52] However, it is in poor agreement with the 0.27 yield determined by Hasson *et al.* (2001).[49] We believe the discrepancy is due to the fact that HCOOH and H_2O_2 were not counted as CH_2OO + $(H_2O)_n$ products in the Hasson *et al.* (2001) work, and the offline HMHP determination may have experienced aqueous losses. The CH_2OO yield reported here is supported by independent observations of its co-products, MVK and MACR (Fig. 1). Fig. 3C shows that the CH_2OO yield determined here is in good agreement with the C_4 carbonyl sum at high water vapor mixing ratios where CH_2OO is fully scavenged. The inferred CH_2OO yield in our work does not include formaldehyde as a product due to limited data. Formaldehyde formation becomes important at low RH because of competing reactions such as CH_2OO + O_3; thus, a significant deviation in the inferred CH_2OO yield compared to the C_4 carbonyl sum occurs in the low RH range.

The products derived from CH_2OO bimolecular reactions have a strong relationship with water vapor mixing ratio due to competition from the CH_2OO + $(H_2O)_n$ reaction (Fig. 3B). Hydroperoxy methylformate (HPMF), seemingly the sole product of the CH_2OO + HCOOH reaction (Fig. S3, ESI†), is observed only under very dry conditions in accordance with previous reports.[27,53] This is because formic acid in ozonolysis experiments is rarely present at the levels needed to compete with water vapor. In addition to compounds reported in Table 1, RH-dependent yields of minor species like acetic acid were also observed (<0.06). Representative CIMS mass spectra showing all products are given in Fig. S4 (ESI†). Acetic acid has not been identified in past isoprene ozonolysis studies, but serves as an important clue in deducing the fragmentation patterns of C_4 Criegees.

HMHP is the most abundant CH_2OO + $(H_2O)_n$ product, followed by formic acid, then H_2O_2 (+ HCHO). The maximum HMHP yield is determined to be ~44% from isoprene (~73% from CH_2OO), somewhat higher than other values reported in the literature. Insightful comparisons with literature values prove challenging, however, due to the poor agreement in CH_2OO + $(H_2O)_n$ product yields. For example, single-point "humid" HMHP and H_2O_2 yields are reported to be 0.09–0.30 and 0.01–0.12, respectively.[27,49,50,54,55] Some of the inconsistencies in past experiments have been attributed to the challenge of quantifying hydroperoxides with offline aqueous methods (*e.g.*, high-performance liquid chromatography (HPLC)).

Interestingly, we find HMHP yields decrease above RH ~ 40% (Fig. 3B). The reduction in yield for HMHP at high humidity is almost fully compensated by an increase in yield for HCOOH (Fig. 3D). Although wall-mediated reaction is a convenient explanation, our RH-dependent corrections for wall loss using authentic compounds should account for this chemistry (Fig. S2, ESI†). Instead, model simulation results in Section 3.2 support the idea that the RH-dependent yields of HMHP and HCOOH are controlled by reactions of both the water monomer and dimer. The dimer becomes exceedingly more abundant at higher RH. As the model simulations fit concentration data that have been wall-loss corrected, the heterogeneous reaction is not included in the mechanism. The atmospherically-relevant reaction of water dimer with CH_2OO was first suggested by Ryzhkov and Ariya[18,21,28] and later confirmed by experimental works.[19,20] Ryzhkov and Ariya suggested the decomposition products to be H_2O_2 and HCHO; however, our data are more consistent with HCOOH as the major product from this reaction.

Past studies explored a large range in water vapor mixing ratio (9000–20 000 ppm, RH ~ 28–63% at 298 K) while reporting only a single 'humid' yield for products. Thus, it is possible that poor literature agreement may be due to snap-shot observations along different humidity points in the HMHP yield curve. These disagreements are likely exacerbated by the absence of wall loss corrections, which depend on the reaction vessel.

To our knowledge, only two other HMHP yield studies have been performed at multiple RH conditions.[24,49] Hasson *et al.* (2001) and Huang *et al.* (2013) did not report yield trends similar to this work, *i.e.*, their data reported a rise-to-maximum relationship of HMHP with RH (maximum yields of 16% and 25%, respectively). Yet, despite the fitting function used by Hasson *et al.* (2001), their data show that the average HMHP yield at RH ~ 80% (~0.12 ± 0.03) is lower than its yield at RH ~ 40% (~0.16 ± 0.04) for isoprene – congruent with our observed trends.

We are unsure of the reasons for discrepancies with the Huang *et al.* (2013) work. In addition to the plateauing HMHP yield, Huang *et al.* (2013) reported a declining yield of HCOOH with humidity (*e.g.*, 40% yield of HCOOH at RH 5% that decreases to 30% yield at RH 90%). It is difficult to understand how HCOOH can be produced in higher yields under dry conditions when HCOOH formation from Criegee isomerization is minor compared to the major channel of $CH_2OO + (H_2O)_n$.[56,57] Again, given the lower HMHP yields reported by studies using offline analysis techniques, it is possible that aqueous losses may have occurred and direct comparisons are not possible. Furthermore, the bis-hydroxymethyl peroxide (BHMP) reported in Huang *et al.* (2013) (and absent in this work) may hint at side reactions that are symptomatic of the high reagent concentrations (ppm level) used in that work or condensed-phase chemistry of H_2O_2 and HCHO.

3.2. Toward a unifying mechanism

Major atmospheric models either do not represent ozonolysis chemistry or provide a significantly abridged version that generally neglects the formation of major compounds such as HMHP.[58,59] Here, we describe a detailed chemical mechanism based on the new data presented in this work and those available in the literature. The *in situ* observations of oxygenated volatile organic compounds and HO_x enable us to place new constraints on many aspects of the mechanism. Mechanism simulations of HCHO assumes that are no observational interferences from ROOH or other compounds, which is currently unverified for the LIF instrument used here but has been identified for proton-transfer-reaction (PTR-) and GC-based instruments.[60] The proposed mechanism provides enough chemical specificity to capture the RH-dependent yields of OH, carbonyls (HCHO, MACR, MVK), and major products of $CH_2OO + (H_2O)_n$ chemistry. Although uncertainties persist along several channels in the ozonolysis chemistry, especially in the fate of the C_4 Criegees, the proposed scheme is a good starting point for further development and use in atmospheric models.

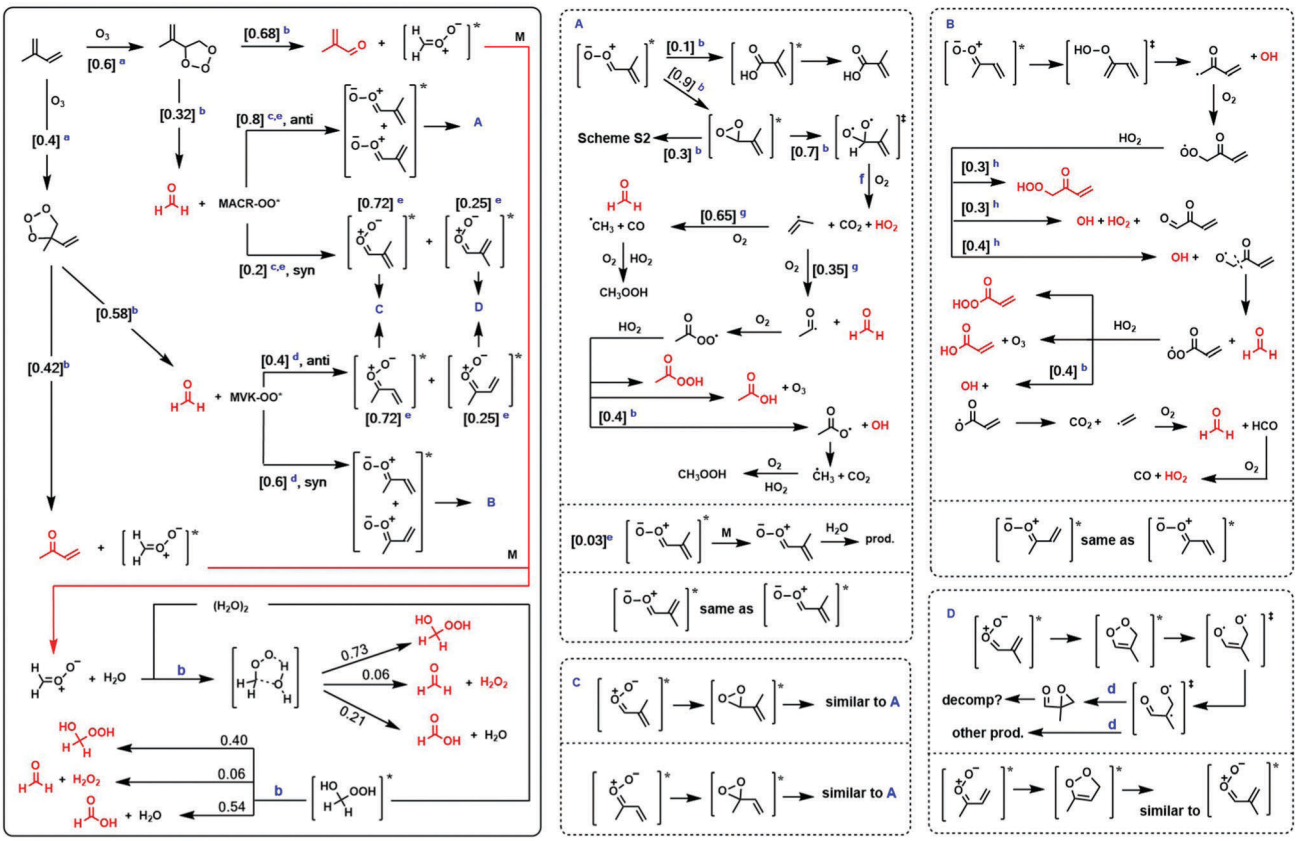

Fig. 4 Overall scheme of isoprene ozonolysis and reactions of Criegee intermediates, with proposed isomerization and decomposition pathways of C_4 Criegees. Observed product species are shown in red. The reaction of CH_2OO with O_3 and isoprene, although present in the model mechanism, are not shown in the figure. Literature values: [a] ref. 8, [b] this work, [c] ref. 61, [d] ref. 62, [e] ref. 5, [f] ref. 63–65, [g] ref. 66, [h] ref. 67.

3.2.1. POZ and C_4 Criegee reactions. Fig. 4 shows the proposed reaction scheme for isoprene ozonolysis. Compounds observed in this work are shown in red. The chemical structures of some of the minor oxygenated species may not be unique, as this CIMS technique cannot distinguish isobaric species. We used the branching ratios for POZ formation that was suggested by Aschmann and Atkinson,[8] which implies that the lower steric hindrance from the 3,4-addition of ozone is more important than the effect of the electron-donating CH_3 group in the 1,2-addition.[61] It is assumed that there is negligible conformational interconversion between Criegees due to their zwitterionic character,[68,69] *i.e.*, the barrier to interconversion is expected to be large.[70] We note that data available for Criegees with allylic groups, which would presumably facilitate interconversion, is still scarce. Thus, the assumptions and reaction channels discussed here may need to be re-evaluated in future work.

Evidence of bimolecular reactions of the C_4 SCI is not significant. For example, the signals of C_4 α-hydroxyalkyl hydroperoxides that are analogous to HMHP, *e.g.*, from the reaction of *anti* MACROO + $(H_2O)_n$, were not observed here. Furthermore, MACR + MVK yields did not significantly increase following SO_2 addition, *e.g.*, as would be expected from the MACROO + SO_2 → MACR + SO_3 reaction. The insignificant production of MACR from the MACROO + SO_2 reaction and the fast *anti*-SCI + H_2O rate coefficient determined recently (2.4×10^{-14} cm^3 $molec^{-1}$ s^{-1})[71] favor the hypothesis that the stabilization fraction of the C_4 Criegees is small, as opposed a larger population of SCI where bimolecular reactions are non-competitive. Thus, we assumed a Criegee stabilization fraction of 0.03 as suggested by Kuwata and Valin.[62] However, accessible unimolecular pathways of CIs and SCIs are often identical, so it is not possible for this study to fully distinguish the two fates. An SCI unimolecular rate constant of ~250 s^{-1} would also be consistent with observations. The 0.03 "stabilization fraction" can be viewed as an effective fraction of Criegees that react bimolecularly under H_2O-dominated conditions. Extensive C_4 Criegee decomposition (hot or thermalized) is consistent with the high yields (>80%) of HCHO that are observed in this work and elsewhere.[48] The production of HCHO from the prompt POZ decomposition is constrained by MVK + MACR yields to be approximately ~40% by mole with respect to isoprene loss. CH_2OO is fully scavenged by water in most of our experiments, so little additional HCHO can originate from side reactions of CH_2OO at atmospherically-relevant RH.

After the POZ decomposition, the distribution of the *syn*/*anti* conformers of the C_4 Criegees is thought to be asymmetric. We used the branching ratios suggested by Kuwata and coworkers,[5,62] with the caveat that the MVK-OO* conformer distribution is loosely based on the hot acetaldehyde oxide, for lack of direct information. Unimolecular reactions of the C_4 Criegees have been suggested to occur *via* 5-member dioxole or 3-member dioxirane intermediates.[5,62,72] The model mechanism allows C_4 Criegees that are *syn* and *anti* to vinyl groups to form dioxole and dioxirane intermediates, respectively, using the theoretically-predicted dioxole/dioxirane branching ratios.[62] Dioxoles have been suggested to isomerize into products containing carbonyl and epoxide functional groups, which may further decompose;[5] however, the CIMS technique used in this work is likely not sensitive to these specific compounds. The dioxole products were not traced in the model because they represent an insignificant fraction of the carbon in the mechanism (~3%) and are not thought to impact OH or HCHO yields. A minor fraction of the *anti* MACROO* is allocated toward hot acid formation, yielding methacrylic acid (which may also occur *via* a dioxirane intermediate).[73] The dioxirane channels represent a larger fraction of the carbon in the ozonolysis. We followed the recommendations of Peeters, Vereecken, and coworkers,[63,64] in conjunction with observations derived from acetaldehyde oxide,[65] to assign the majority of the dioxirane fate to the decarboxylation pathway (products CO_2 + HO_2 + alkyl radical for dioxiranes in the primary position). A decarboxylation branching ratio of ~0.7 gave good agreement with observations. As these dioxiranes have allylic functionality, we assign the balance of the carbon to a proposed isomerization pathway (Scheme S2, ESI†) that may form a stable product. The alkyl radical that is produced in the decarboxylation step in Route A is the methylvinyl radical, which is known to generate HCHO + peroxyacetyl radical (~0.35) or HCHO + methylperoxyl radical + CO (~0.65) in the presence of oxygen.[66] It is probable that the observed acetic acid (0.02–0.06 from dry to humid) is produced from the reaction of peroxyacetyl radicals with HO_2 or RO_2.[74–77] We speculate that the higher acetic acid yield under more humid conditions may be due to unidentified wall reactions. The methylperoxyl radical is a precursor to methyl hydroperoxide under HO_2-dominant conditions. Methyl hydroperoxide has been identified in previous works,[50,78] but without complete mechanistic knowledge of its chemical source.

The *syn* MVKOO* will decompose to OH and a beta-oxy alkyl radical *via* a vinylhydroperoxide intermediate (B route). The further reactions of the beta-oxy alkylperoxyl radical (RO_2) are much more uncertain. In the mechanism suggested here, this chemistry is proposed to proceed similarly to the RO_2 radicals found in MVK + OH chemistry that have analogous functionality.[67] We followed the recommendations in Praske *et al.* (2015) for the branching ratios of the three product channels with HO_2: beta-oxy hydroperoxide, 1,2-dicarbonyl + OH + HO_2, and alkoxyl radical (RO) + OH + O_2. The RO radical fragments to formaldehyde and an acyl radical and promptly reacts with O_2 to produce an acylperoxyl (RC(O)OO) radical. The acylperoxyl radical may undergo three fates upon reaction with HO_2 (Fig. 4B), modeled after reactions of peroxyacetyl.[79,80] These data suggest that decarboxylation is an important fate for this particular acylperoxyl radical, which affects both OH and formaldehyde in the process (*via* the chemistry of the vinyl radical.)[81]

3.2.2. C_1 Criegee + water reaction. The mechanism illustrated in Fig. 4 was integrated into a kinetic model. Most of the rates and branching ratios available in the literature were imported for use in the model mechanism and assumed to be accurate. The product yields and rate coefficients of Criegee reactions labeled [b] in Fig. 4 were empirically tuned to provide satisfactory agreement with observational data within the full RH range, as shown in Fig. 5. The reaction inputs into the kinetic model are shown in Scheme S1 (ESI†). We find that

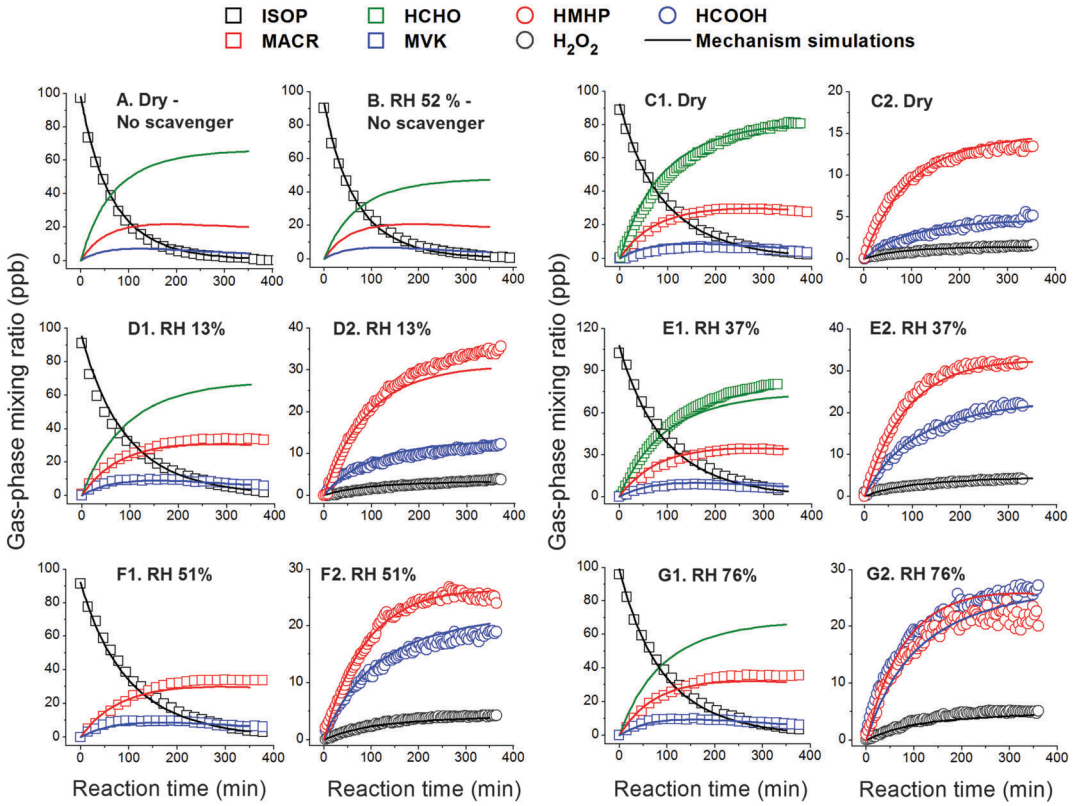

Fig. 5 Panels A–G show the comparison between gas-phase observations from different experiments (various markers) and results from model mechanism simulations based on Fig. 4 (solid lines). Subpanels show the mixing ratios of (1) isoprene and carbonyls and (2) CH_2OO + $(H_2O)_n$ products, when applicable. Simulations under "Dry" conditions used RH = 1.2%. The displayed mixing ratios of HMHP and HCOOH have been corrected for first-order wall loss (Fig. S2, ESI†). The model inputs are shown in Scheme S1 (ESI†). Experimental conditions for the measured data are found in Table 1.

variations in the molar yields of HMHP, HCOOH, HCHO and H_2O_2 with RH can only be simulated if the reaction with water dimer is included in the mechanism. The mixing ratio of water dimers was calculated based on their equilibrium thermodynamics at 295 K (Fig. S5A and B, ESI†).[82]

Some of the observed H_2O_2 in the ozonolysis experiments (Table 1) originates from the HO_2 + HO_2 → H_2O_2 + O_2 reaction (Fig. S6 and Scheme S1, ESI†). Using published rate constants and HO_2 observations we estimate the HO_2 self-reaction accounts for ~50% of the observed H_2O_2. However, considering the uncertainties in the HO_2 and H_2O_2 observations we cannot exclude the possibility that the HO_2 self-reaction explains the entirety of the observed H_2O_2, and thus, that the CH_2OO + $(H_2O)_n$ → H_2O_2 + HCHO channel has zero yield (see error bounds in Fig. S6, ESI†). We adjusted the product branching ratios for the CH_2OO + $(H_2O)_n$ reactions to remove the average contribution from HO_x chemistry, and this is shown in the left-most panel of Fig. 4. The product branching in the dimer reaction favors formic acid formation over HMHP formation, which is consistent with the suggestion that the reaction of CH_2OO with water dimer to form HMHP is exothermic, and some of the excited HMHP produced by that pathway may further decompose (in this case to formic acid + H_2O) with water acting as a catalyst.[28]

We used the following rate coefficients for the reaction of CH_2OO with water in the model mechanism: k_{H_2O} = 9 × 10^{-16} cm^3 $molec^{-1}$ s^{-1} and $k_{(H_2O)_2}$ = 8 × 10^{-13} cm^3 $molec^{-1}$ s^{-1}. The water monomer reaction rate coefficient falls within the upper limit determined by Welz *et al.* (2012)[83] and by other works (<4 × 10^{-15} cm^3 $molec^{-1}$ s^{-1}). The dry (RH ~ 1%) observations provided constraints for the monomer rate coefficient, and the dimer rate coefficient was adjusted until model results satisfactorily reproduces measurements. We found that a dimer reaction coefficient faster than that of the monomer reaction, but slower than the coefficient suggested by some studies (4–6.5 × 10^{-12} cm^3 $molec^{-1}$ s^{-1}),[19,20,84] gave the best fit with the observational results across all RH conditions.

Fig. S7 (ESI†) shows results of a sensitivity study of the water rate coefficients in the model, which concludes that the rate coefficient of Chao *et al.* (2015) is too large to simulate the data in this work. Our suggested dimer rate coefficient of $k_{(H_2O)_2}$ = 8 × 10^{-13} cm^3 $molecule^{-1}$ s^{-1} is consistent with those of Newland *et al.* (2015), who found that 5.6 (±7.0) × 10^{-13} cm^3 $molec^{-1}$ s^{-1} best describe their chamber data. Leather *et al.* (2012) also found the rate coefficient of CH_2OO with "water" to be in the range of ~1 × 10^{-15}–1 × 10^{-12} cm^3 $molec^{-1}$ s^{-1} when measuring HCOOH.[85] HCOOH is the product of both the water monomer and dimer reaction with CH_2OO, so the observed

range is in agreement with this work. The difference between reported CH_2OO + water dimer rate coefficients in the literature is striking, but the source of the disagreement is unclear.

The reaction timescales, Criegee generation methods, reaction vessel characteristics, and Criegee concentrations in literature works are different – all of which may play a role in the discrepancy. Furthermore, if water vapor may intercept the hot Criegee directly during ozonolysis reactions, in a manner analogous to the interception of excited alkyl radicals by O_2,[86] then there may be significant deviations between chamber and direct kinetic determinations as direct determinations produce and investigate SCI preferentially. The result is a promotion of the H_2O reaction over the $(H_2O)_2$ reaction during ozonolysis. Assuming CI interception occurs to a non-negligible extent, observations from chamber studies would be more immediately relevant for atmospheric modeling than current data from direct determinations.

Fig. S5C (ESI†) shows the relative contribution of each reaction using the aforementioned rate coefficients, where the dimer reaction can contribute up to ~65% as the humidity approaches 100%. However, the water monomer reaction is an important sink for CH_2OO under all atmospherically-relevant RH.

3.2.3. OH and HO_2 formation. The production of OH can be visualized from the decay of isoprene in the experiments where an OH scavenger was not present (Fig. 5A and B). OH was directly measured by LIF; however, the high dilution ratio used in the laboratory to conserve chamber volume degraded the signal-to-noise of the instrument. In addition, the experimental conditions in the reaction (including high peroxide mixing ratios) and unknown interferences that may be related to unsaturated hydrocarbon + ozone chemistry[35,87] resulted in uncertainty bounds in the direct OH determination that were too high to constrain yields. Thus, a combination of modeling and isoprene decay measurements was used to estimate [OH]. Estimations of OH sources in the model mechanism relied on constraints provided by other products. An overall OH yield of approximately 28(±5)% gives good agreement with observations under both dry and humid conditions, *e.g.*, the comparison between observed and simulated isoprene decays produced least-squares slope = 1.023, R^2 = 0.999 at RH < 4% and slope = 1.015, R^2 = 0.998 at RH 52%, and is consistent with the recommended value by IUPAC (25%).[1] It should be noted that not all of this OH is produced from the prompt VHP channel. This would necessitate almost 100% *syn* branching for MVKOO* and for the following radical chemistry to be OH neutral. Instead, the constraints placed by closed-shell products in the mechanism predict that prompt decomposition (from *syn*-MVKOO*) accounts for a 14% yield of OH, with respect to the reaction of isoprene, and further chemistry of the beta-oxy alkyl radical generates another 12%. The remaining minor fraction arises from unimolecular reactions of the C_4 Criegees. Neither the POZ decomposition nor the following RO_2 chemistry is expected to be sensitive to water vapor, in good agreement with the stable OH yields between dry and humid conditions. Our OH source contribution results are fairly consistent with those using a statistical-dynamical master equation and transition state theory, which predicts an OH prompt production yield of 11% for a total yield of 25%.[61]

HO_2 is generated and consumed along various reaction channels in ozonolysis (Fig. 4). The HO_x cycling of OH and HO_2 also occurs in conjunction with ozonolysis in the model mechanism (Scheme S1, ESI†). Major sources of HO_2 from ozonolysis include decarboxylation of primary dioxiranes (Route A) and the further chemistry of the beta-oxy alkyl radical (Route B). A major sink of HO_2 in this work is the reaction with the RO_2 radical produced from cyclohexane (OH scavenger). As a result, the usage of other OH scavengers may change the HO_2 concentrations during similar experiments. Fig. S8 (ESI†) shows that HO_2 simulated using the kinetic model shown in Scheme S1 (ESI†) agrees fairly well with the measured values under dry and humid conditions at the start of the reaction (~40 ppt). As the reaction progresses, however, the agreement worsens (simulated HO_2 is lower than measured.) We believe this is because the simulated scheme does not trace second generation products, which appear to produce a significant quantity of HO_2.

3.2.4. HCHO formation. The difference in observed HCHO between the dry (RH ~ 1% in the simulation) and RH 37% experiments provides unique insights into the bimolecular reaction of CH_2OO (Fig. 5, Panels C1 and E1). The model predicts that a non-negligible fraction of HCHO can be produced from the CH_2OO reaction with ozone,[13,88] the second most abundant reaction partner for CH_2OO in our experiments, when the reaction conditions are dry. For $k_{CH_2OO+O_3} \sim 1 \times 10^{-12}$ cm^3 molec^{-1} s^{-1}, as has been previously suggested,[16] the best fit with observations is achieved by assuming a formaldehyde yield of 0.7 (while conserving a faster rate), instead of the recommended value of 1. While it is possible that unknown pathways for the CH_2OO + O_3 reaction exist, we believe it more likely that the model mechanism is missing a Criegee sink that is ~30% of the effective CH_2OO + O_3 reaction, but does not produce HCHO, when the reaction is performed dry. If a missing sink exists, it is not the Criegee self-reaction, as including even the fastest experimentally-determined rate coefficient[89] did not alter the simulations. All side reactions of CH_2OO become negligible when RH reaches atmospherically-relevant levels. Of the HCHO sources discussed in this work that are important under atmospherically-relevant conditions, the initial POZ decomposition comprises the majority production pathway (~60%). The model simulations predict that unimolecular reactions of C_4 Criegees to contribute another relative ~35% and the reaction of CH_2OO + $(H_2O)_n$ is a relatively small (~5%) source of formaldehyde. As we noted above, the yield of HCHO and H_2O_2 from this channel could be zero within uncertainties.

3.2.5. Other reactions of the C_1 Criegee. Finally, we use the RO_2 + CH_2OO rate coefficient of Vereecken *et al.* (2012) ($k \sim 5 \times 10^{-12}$ cm^3 molec^{-1} s^{-1})[15] and the OH reaction kinetics for cyclohexane[1] to examine whether the 50 ppm of OH scrubber produces enough RO_2 to impact CH_2OO yields in the ozonolysis reaction. The model results suggest that cyclohexane RO_2 radicals were not competitive with water as a Criegee scavenger during the experiments in this work. In addition, inserting the

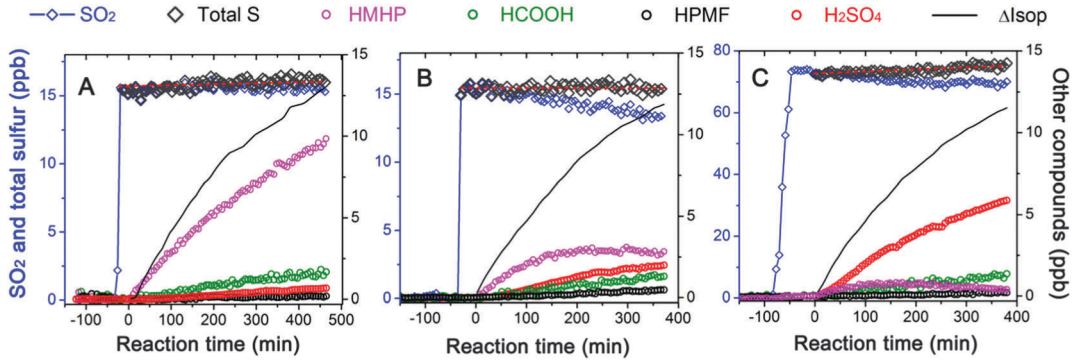

Fig. 6 Relative rate experiments of H_2O and SO_2 as scavengers for CH_2OO, produced by the ozonolysis of ~20 ppbv of isoprene at 298 K, under the following conditions: (A) 15 ppbv of SO_2 and 20% RH, (B) 15 ppbv of SO_2 and <4% RH, and (C) 75 ppbv of SO_2 and <4% RH. Total sulfur (black diamonds) represents the sum of SO_2 and H_2SO_4.

reaction of isoprene + CH_2OO into the model mechanism ($k = 1.78 \times 10^{-13}$ cm^3 molec^{-1} s^{-1}),[16] as suggested by Vereecken *et al.* (2014), did not significantly perturb the model simulation results. However, in studies where initial isoprene and ozone are present at ppm levels, the CH_2OO + alkene reaction may play a bigger role. These newly-identified reactions may be one source of discrepancy in literature yield data, underscoring the importance of using atmospherically-relevant mixing ratios of reactants or verifying that secondary chemistry is not affecting laboratory results.

3.3. Competitive rates of CH_2OO + $(H_2O)_n$ and CH_2OO + SO_2

Although water reactions are thought to dominate the fate of CH_2OO in the atmosphere,[11,19,20,28,32] it has been suggested that the reaction of SCI with SO_2 may be important from the perspective of H_2SO_4 production and, thus, particle formation.[90] Here, we measure the competitive rates of the reaction of isoprene SCIs with H_2O and SO_2, using isoprene mixing ratios that approach atmospheric levels (~20 ppb) and realistic concentrations of SO_2. This measurement is sensitive to the combined effects of CH_2OO and the C_4 SCIs of isoprene. However, it is clear that the dominant fraction of the bimolecular reactivity originates from CH_2OO, illustrated by the similar SCI yields when using SO_2 as a scavenger compared to H_2O (Table 1). Notably, the orders of magnitude uncertainties that exist in the absolute rate coefficients for CH_2OO bimolecular reactions[17,28,62,83,91–94] become immaterial when determining relative rates.

Fig. 6 shows the reaction progress for three relative rate experiments between H_2O and SO_2 during an isoprene ozonolysis performed with an OH scavenger. At 15 ppb of SO_2 and 20% RH, representative of a dry and polluted day, greater than 90% of CH_2OO reacted with water as evidenced by the large abundance of HMHP and HCOOH as compared to H_2SO_4 (Fig. 6A). Only under the driest conditions (RH < 4%) does CH_2OO appreciably oxidize SO_2 at initial levels of ~15 ppb (Fig. 6B). Although under these conditions, the water reaction is still the major reaction pathway for CH_2OO. Here, we start to witness decreasing mixing ratios of HMHP with time, which is due to heterogeneous loss on acidic surfaces from the H_2SO_4 production and is uncorrected in Fig. 6. Only under exceptionally dry (RH < 4%) and exceptionally high $[SO_2]_0$ (~75 ppb) conditions does SO_2 oxidation become the dominant fate of CH_2OO (Fig. 6C), although these specific conditions are rarely found on Earth.

The relative rate of $k_{SO_2}/k_{(H_2O)_n} = 2.2\ (\pm 0.3) \times 10^4$ determined from the data is in good agreement with the $k_{SO_2}/k_{(H_2O)_n}$ range of $(1–3) \times 10^4$ reported in other studies.[32,83,92] However, these results are considerably different than those of Stone *et al.* (2014),[93] who measured a lower limit of $k_{SO_2}/k_{(H_2O)_n} > 4 \times 10^5$. Although the source of the discrepancy is not clear, the experiments of Stone *et al.* (2014) were performed differently compared to this work. Stone *et al.* (2014) quantified CH_2OO decay *via* chemical scavenging to form HCHO and made the assumption that HCHO production is proportional to CH_2I (Criegee precursor) concentrations. Like other studies that measure CH_2OO decay,[95] Stone *et al.* (2014) provides lower limits on $k_{SO_2}/k_{(H_2O)_n}$ due to unknown processes that affect the first-order SCI decay when H_2O is added. As this work captures at least one co-product of each branch in the CH_2OO + $(H_2O)_n$ reaction, our measurement can be considered absolute. However, it must be noted that challenges in quantifying low $[H_2O]$ and complex reaction products also give rise to significant uncertainties in this work – a limitation that likely permeates all studies of SCI + $(H_2O)_n$ reactions.

3.4. Fates of CH_2OO in the atmosphere – a case study from SOAS

To put the competition between the reaction of H_2O and SO_2 with CH_2OO into perspective, it would require 500 ppb of SO_2 to have equal reactivity with H_2O at an average RH of 30% (T = 295 K, P = 1 atm). Many areas of the world are more humid than this RH level, especially in forested areas where biogenic emissions are high. At RH > 50%, the amount of SO_2 needed for equal reactivity would be found only in a power plant or volcanic plume. Here, we examine the fates of CH_2OO and molecular contributors to SO_2 oxidation in a typical Southeastern United States forest that emits predominantly isoprene during summer. The comprehensive datasets were obtained by multiple investigators as part of the Southern Oxidant and Aerosol Study in Brent, AL during June of 2013 (https://soas2013.rutgers.edu/). A time-of-flight CF_3O^- CIMS provided

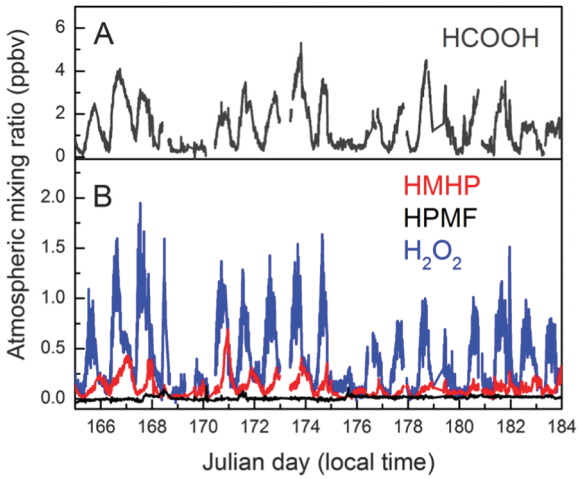

Fig. 7 Measurements of compounds that are formed *via* CH_2OO bimolecular reactions during the SOAS 2013 campaign (A) formic acid, and (B) HMHP, HPMF, and H_2O_2. HCOOH and H_2O_2, in particular, have multiple photochemical sources.

measurements of SO_2, H_2O_2, and oxidized organic compounds and a commercial weather station (Coastal Environmental Systems model Zeno 3200) provided measurements of T, P, and RH needed to calculate water vapor mixing ratio. The measurement site was occasionally impacted by SO_2 pollution from nearby power plants.

Fig. 7 shows the measured CH_2OO + $(H_2O)_n$ products and the CH_2OO + HCOOH product for the duration of the SOAS study. While HCOOH and H_2O_2, two compounds with multiple photochemical sources, are known to have high concentrations at the Earth's surface, the presence of large abundances of HMHP produced from biogenic ozonolysis chemistry has previously not been fully appreciated. The mixing ratio of HMHP reaches 600 ppt during some events at this site (Fig. 7B). Other limited observations of HMHP report even higher mixing ratios.[96] Concentrations of HMHP are comparable to the sum of two major products of the isoprene + OH oxidation under HO_2-dominated conditions (ISOPOOH + IEPOX) during the SOAS campaign.[44] We note, however, that the interpretation of the ambient surface mixing ratio of HMHP is challenging as it is affected by poorly-constrained oxidative and photolytic loss processes. Additionally, the nocturnal peak concentrations of HMHP reflect both chemical production and nighttime boundary layer dynamics.

The persistently humid (2–3 vol% H_2O) and occasionally polluted atmosphere at SOAS provides a useful case study to examine the reactions of CH_2OO (Fig. S9A and B, ESI†). Despite plumes that approached 10 ppb, SO_2 only negligibly impacted the CH_2OO fate. Using laboratory-derived relative rate results (Section 3.3), CH_2OO loss in the gas phase was almost entirely controlled by the H_2O reactions (>98%) for every day of the SOAS study (Fig. S10A, ESI†). At peak SO_2 mixing ratios, the fraction of CH_2OO that was oxidized by SO_2 was below 1%. In comparison, the effective reaction with HCOOH is slightly more efficient at 1–2% of the total CH_2OO fate due to high HCOOH mixing ratios (~4 ppb, Fig. 7A) and a faster rate coefficient (k_{HCOOH}/k_{SO_2} ~ 2.8).[52] Still, the product of the CH_2OO + HCOOH reaction, HPMF, was not present at quantifiable concentrations during the majority of the month-long study (Fig. 7B). Using peak SO_2 and HCOOH mixing ratios observed during the SOAS campaign, we find that the water reaction is dominant at all atmospherically-relevant RH (Fig. S10B, ESI†).

Given the ubiquity of water in the troposphere, it is more informative to explore the CH_2OO reactions from the point of view of SO_2 and HCOOH oxidation. We use the observed mixing ratios of ozone, abundant exocyclic alkenes (isoprene and β-pinene), and water vapor to estimate the steady-state concentrations of CH_2OO at this site (~2×10^3 molec cm^3 in the daytime) for the month-long study (Fig. S8, ESI†). The production term was calculated from the ozonolysis reaction, using respective SCI yields of 0.6 for isoprene (this work) and 0.3 for β-pinene (assuming that the scavenged SCI are mostly CH_2OO).[49] The loss term assumes H_2O and $(H_2O)_2$ are the only sinks for CH_2OO at this site (Fig. S10B, ESI†). α-Pinene is the second most abundant alkene in this forest but its ozonolysis is not thought to produce CH_2OO. The rate coefficients of relevant reactions[1,97] were calculated using measured temperature inputs (292–306 K) during SOAS: k_{ISO+O_3} (~1×10^{-17}cm^3 molec^{-1} s^{-1}), k_{BPIN+O_3} (~2×10^{-17} cm^3 molec^{-1} s^{-1}), k_{OH+SO_2} (~1×10^{-12} cm^3 molec^{-1} s^{-1}), and $k_{OH+HCOOH}$ (~4.5×10^{-13} cm^3 molec^{-1} s^{-1}). The average OH concentration used in the calculation was 1×10^6 molec cm^{-3}. For CH_2OO reaction coefficients, we used $k_{SO_2}/k_{(H_2O)_n}$ ~ 2.2×10^4 (where n = 1, 2; this work), absolute rate coefficients as reported in Section 3.2.2, and two different relative rate determinations for HCOOH reactions that are notably different: k_{HCOOH}/k_{SO_2} ~ 2.8 ("k_{HCOOH} 1")[52] and $k_{HCOOH}/k_{(H_2O)}$ ~ 1.4×10^4 ("k_{HCOOH} 2").[27]

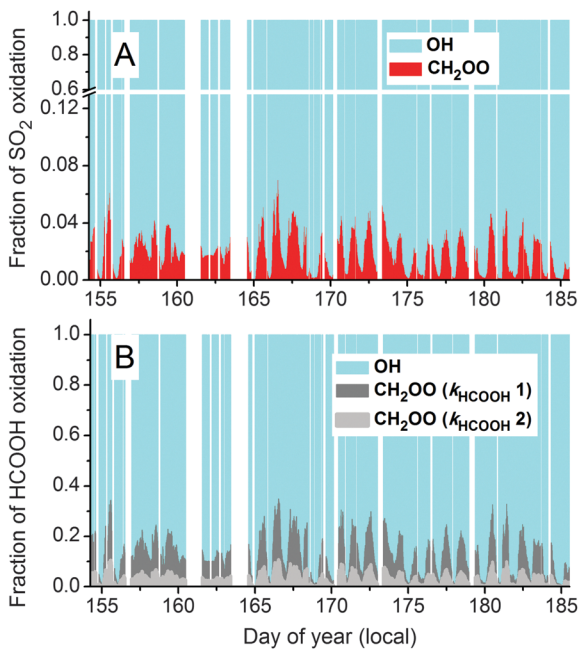

Fig. 8 Significance of CH_2OO as an oxidant for (A) SO_2 and (B) HCOOH. In panel B, relative rate determinations by (1) Sipila *et al.* (2014) and (2) Neeb *et al.* (1997) were used.

Using $k_{SO_2}/k_{(H_2O)_n}$ and $k_{(H_2O)}$ in this work, $k_{HCOOH\ 1} \approx 5.5 \times 10^{-11}$ cm^3 molec^{-1} s^{-1} and $k_{HCOOH\ 2} \approx 2.0 \times 10^{-11}$ cm^3 molec^{-1} s^{-1}.

Fig. 8A shows that CH_2OO accounts for $<6\%$ of the gas-phase SO_2 oxidation at the SOAS site. This is in stark contrast to the proposed 50% contribution of "compound X" (suggested to be related to Criegee chemistry) to the oxidation of SO_2 in a Finnish boreal forest.[90] The discrepancy has been suggested to be due to the different distribution of volatile alkenes in boreal forests, *i.e.*, that the SCI from α-pinene may have a higher relative contribution to SO_2 oxidation. However, given the large OH yields from α-pinene ozonolysis (0.70–0.91),[98–102] and the fast decomposition rates of larger Criegees (this work and elsewhere), the population of SCIs that are available for bimolecular reaction from α-pinene is expected to be small and their contribution to sulfate formation, thus, an open question. In cleaner environments, a significant pathway toward new particle formation may be the production of extremely low volatility compounds from α-pinene ozonolysis,[103,104] through the VHP channel and subsequent autoxidation reactions[105] of the RO_2. In comparison, CH_2OO may oxidize a larger amount ($<35\%$) of HCOOH, as its CH_2OO reaction is faster and its OH reaction is slower than the analogous reactions for SO_2. However, depositional losses, instead of oxidation, is thought to dominate the atmospheric fate of HCOOH ($\tau_{dep} \sim$ 20–40 h (at 1.5 km PBL height), $\tau_{OH} \sim$ 620 h, $\tau_{SCI} \sim$ 1800 h).[44] Finally, we conclude that CH_2OO does not significantly affect the atmospheric lifetime of SO_2 or HCOOH.

4. Atmospheric implications

This work provides new insights into the reactions of isoprene-derived Criegee intermediates, especially for the decomposition pathways of the excited C_4 Criegees where scarce experimental data are available. The model mechanism in this work suggests that C_4 Criegees decompose to OH, HCHO, and other products in the atmosphere without significantly producing SCI that participate in bimolecular reactions. Some existing atmospheric models, such as the Master Chemical Mechanism (MCM), assume the C_4 Criegees lose $O(^3P)$ to form MVK and MACR, although this is not supported by our observations. A significant portion of the OH and HCHO yields is secondary. One reaction, subset $CH_2OO + (H_2O)_n$, accounts for almost all of the SCI bimolecular reactions in isoprene ozonolysis under typical atmospheric conditions. This implies that isoprene-derived SCIs are a negligible contributor to H_2SO_4 production in the atmosphere. If stabilized Criegees indeed play a role in new particle formation, the events will be localized to regions that are not dominated by the reactivity of ozone with isoprene. Those areas may instead be abundant in the small hydroperoxides that are quickly deposited to plant canopies.[44] Our data are consistent with the suggestion that isoprene emissions can suppress new particle formation,[106] although the specific inhibition mechanism is still unclear, while these events readily occur in boreal forests.[107] Discussions of whether monoterpene SCI in Boreal forests may appreciably oxidize SO_2 will hinge on the understanding of their unimolecular lifetimes and $(H_2O)_n$ reactivity. Lastly, due to the structurally-specific reactivities of SCI, model simulations of ozonolysis chemistry should explicitly speciate alkenes and incorporate a conformationally-dependent reaction scheme. Incorporation of the isoprene ozonolysis mechanism (Fig. 4 and Scheme S1, ESI†) into atmospheric models will likely improve the accuracy of OH, HO_2, and trace gas simulations in the atmosphere.

Acknowledgements

Funding for this work was provided by the U.S. National Science Foundation (NSF) Postdoctoral Research Fellowship award AGS-1331360, NSF grant AGS-1240604, and the Electric Power Research Institute grant EPRI-10003903. We thank the organizers and participants of the FIXCIT chamber campaign and SOAS field campaign.

References

1 R. Atkinson, D. L. Baulch, R. A. Cox, J. N. Crowley, R. F. Hampson, R. G. Hynes, M. E. Jenkin, M. J. Rossi, J. Troe and I. Subcommittee, *Atmos. Chem. Phys.*, 2006, **6**, 3625–4055.
2 R. Criegee, *Angew. Chem., Int. Ed. Engl.*, 1975, **87**, 765–771.
3 J. H. Kroll, S. R. Sahay, J. G. Anderson, K. L. Demerjian and N. M. Donahue, *J. Phys. Chem. A*, 2001, **105**, 4446–4457.
4 G. T. Drozd and N. M. Donahue, *J. Phys. Chem. A*, 2011, **115**, 4381–4387.
5 K. T. Kuwata, M. R. Hermes, M. J. Carlson and C. K. Zogg, *J. Phys. Chem. A*, 2010, **114**, 9192–9204.
6 N. M. Donahue, G. T. Drozd, S. A. Epstein, A. A. Presto and J. H. Kroll, *Phys. Chem. Chem. Phys.*, 2011, **13**, 10848–10857.
7 S. E. Paulson, R. C. Flagan and J. H. Seinfeld, *Int. J. Chem. Kinet.*, 1992, **24**, 103–125.
8 S. M. Aschmann and R. Atkinson, *Environ. Sci. Technol.*, 1994, **28**, 1539–1542.
9 R. Gutbrod, E. Kraka, R. N. Schindler and D. Cremer, *J. Am. Chem. Soc.*, 1997, **119**, 7330–7342.
10 P. Neeb, O. Horie and G. K. Moortgat, *J. Phys. Chem. A*, 1998, **102**, 6778–6785.
11 J. D. Fenske, A. S. Hasson, A. W. Ho and S. E. Paulson, *J. Phys. Chem. A*, 2000, **104**, 9921–9932.
12 D. Johnson and G. Marston, *Chem. Soc. Rev.*, 2008, **37**, 699–716.
13 H. G. Kjaergaard, T. Kurtén, L. B. Nielsen, S. Jørgensen and P. O. Wennberg, *J. Phys. Chem. Lett.*, 2013, **4**, 2525–2529.
14 S. Hatakeyama and H. Akimoto, *Res. Chem. Intermed.*, 1994, **20**, 503–524.
15 L. Vereecken, H. Harder and A. Novelli, *Phys. Chem. Chem. Phys.*, 2012, **14**, 14682–14695.
16 L. Vereecken, H. Harder and A. Novelli, *Phys. Chem. Chem. Phys.*, 2014, **16**, 4039–4049.
17 J. M. Anglada, J. Gonzalez and M. Torrent-Sucarrat, *Phys. Chem. Chem. Phys.*, 2011, **13**, 13034–13045.
18 A. B. Ryzhkov and P. A. Ariya, *Chem. Phys. Lett.*, 2002, **367**, 423–429.

19 T. Berndt, J. Voigtländer, F. Stratmann, H. Junninen, R. L. Mauldin III, M. Sipilä, M. Kulmala and H. Herrmann, *Phys. Chem. Chem. Phys.*, 2014, **16**, 19130–19136.
20 W. Chao, J.-T. Hsieh, C.-H. Chang and J. J.-M. Lin, *Science*, 2015, 1261549.
21 A. B. Ryzhkov and P. A. Ariya, *Chem. Phys. Lett.*, 2006, **419**, 479–485.
22 O. Horie, P. Neeb, S. Limbach and G. K. Moortgat, *Geophys. Res. Lett.*, 1994, **21**, 1523–1526.
23 P. Neeb, O. Horie and G. K. Moortgat, *Chem. Phys. Lett.*, 1995, **246**, 150–156.
24 D. Huang, Z. Chen, Y. Zhao and H. Liang, *Atmos. Chem. Phys.*, 2013, **13**, 5671–5683.
25 S. Gäb, E. Hellpointner, W. V. Turner and F. Korte, *Nature*, 1985, **316**, 535–536.
26 K. H. Becker, J. Bechara and K. J. Brockmann, *Atmos. Environ.*, 1993, **27**, 57–61.
27 P. Neeb, F. Sauer, O. Horie and G. K. Moortgat, *Atmos. Environ.*, 1997, **31**, 1417–1423.
28 A. B. Ryzhkov and P. A. Ariya, *Phys. Chem. Chem. Phys.*, 2004, **6**, 5042–5050.
29 J. Thamm, S. Wolff, W. V. Turner, S. Gäb, W. Thomas, F. Zabel, E. H. Fink and K. H. Becker, *Chem. Phys. Lett.*, 1996, **258**, 155–158.
30 S. Hatakeyama, H. Kobayashi and H. Akimoto, *J. Phys. Chem.*, 1984, **88**, 4736–4739.
31 A. Novelli, L. Vereecken, J. Lelieveld and H. Harder, *Phys. Chem. Chem. Phys.*, 2014, **16**, 19941–19951.
32 M. J. Newland, A. R. Rickard, M. S. Alam, L. Vereecken, A. Muñoz, M. Ródenas and W. J. Bloss, *Phys. Chem. Chem. Phys.*, 2015, **17**, 4076–4088.
33 H.-L. Huang, W. Chao and J. J.-M. Lin, *Proc. Natl. Acad. Sci. U. S. A.*, 2015, **112**, 10857–10862.
34 M. Olzmann, E. Kraka, D. Cremer, R. Gutbrod and S. Andersson, *J. Phys. Chem. A*, 1997, **101**, 9421–9429.
35 T. B. Nguyen, J. D. Crounse, R. H. Schwantes, A. P. Teng, K. H. Bates, X. Zhang, J. M. St. Clair, W. H. Brune, G. S. Tyndall, F. N. Keutsch, J. H. Seinfeld and P. O. Wennberg, *Atmos. Chem. Phys.*, 2014, **14**, 13531–13549.
36 S. W. Sharpe, R. L. Sams and T. J. Johnson, The PNNL quantitative IR database for infrared remote sensing and hyperspectral imaging, *Proceedings of the 31st Applied Imagery Pattern Recognition Workshop (AIPRí02)*, 2002, DOI: 10.1109/aipr.2002.1182253.
37 F. Drewnick, S. Hings, P. DeCarlo, J. Jayne, M. Gonin, K. Fuhrer, S. Weimer, J. Jimenez, K. Demerjian, S. Borrmann and D. Worsnop, *Aerosol Sci. Technol.*, 2005, **39**, 637–658.
38 J. R. Hottle, A. J. Huisman, J. P. DiGangi, A. Kammrath, M. M. Galloway, K. L. Coens and F. N. Keutsch, *Environ. Sci. Technol.*, 2009, **43**, 790–795.
39 J. DiGangi, E. Boyle, T. Karl, P. Harley, A. Turnipseed, S. Kim, C. Cantrell, R. Maudlin Iii, W. Zheng and F. Flocke, *Atmos. Chem. Phys.*, 2011, **11**, 10565–10578.
40 W. H. Brune, P. S. Stevens and J. H. Mather, *J. Atmos. Sci.*, 1995, **52**, 3328–3336.
41 H. Fuchs, B. Bohn, A. Hofzumahaus, F. Holland, K. Lu, S. Nehr, F. Rohrer and A. Wahner, *Atmos. Meas. Tech.*, 2011, **4**, 1209–1225.
42 J. D. Crounse, K. A. McKinney, A. J. Kwan and P. O. Wennberg, *Anal. Chem.*, 2006, **78**, 6726–6732.
43 J. M. St. Clair, D. C. McCabe, J. D. Crounse, U. Steiner and P. O. Wennberg, *Rev. Sci. Instrum.*, 2010, **81**, 094102.
44 T. B. Nguyen, J. D. Crounse, A. P. Teng, J. M. St. Clair, F. Paulot, G. M. Wolfe and P. O. Wennberg, *Proc. Natl. Acad. Sci. U. S. A.*, 2015, **112**, E392–E401.
45 H. Niki, P. D. Maker, C. M. Savage and L. P. Breitenbach, *Chem. Phys. Lett.*, 1980, **75**, 533–535.
46 T. Su and W. J. Chesnavich, *J. Chem. Phys.*, 1982, **76**, 5183–5185.
47 A. S. Hasson, M. Y. Chung, K. T. Kuwata, A. D. Converse, D. Krohn and S. E. Paulson, *J. Phys. Chem. A*, 2003, **107**, 6176–6182.
48 D. Grosjean, E. L. Williams and E. Grosjean, *Environ. Sci. Technol.*, 1993, **27**, 830–840.
49 A. S. Hasson, A. W. Ho, K. T. Kuwata and S. E. Paulson, *J. Geophys. Res.*, 2001, **106**, 34143–34153.
50 F. Sauer, C. Schäfer, P. Neeb, O. Horie and G. K. Moortgat, *Atmos. Environ.*, 1999, **33**, 229–241.
51 R. Atkinson, S. M. Aschmann, J. Arey and B. Shorees, *J. Geophys. Res.*, 1992, **97**, 6065–6073, DOI: 6010.1029/6092JD00062.
52 M. Sipilä, T. Jokinen, T. Berndt, S. Richters, R. Makkonen, N. M. Donahue, R. L. Mauldin Iii, T. Kurtén, P. Paasonen, N. Sarnela, M. Ehn, H. Junninen, M. P. Rissanen, J. Thornton, F. Stratmann, H. Herrmann, D. R. Worsnop, M. Kulmala, V. M. Kerminen and T. Petäjä, *Atmos. Chem. Phys.*, 2014, **14**, 12143–12153.
53 A. S. Hasson, G. Orzechowska and S. E. Paulson, *J. Geophys. Res.*, 2001, **106**, 34131–34142.
54 K. H. Becker, K. J. Brockmann and J. Bechara, *Nature*, 1990, **346**, 256–258.
55 R. Simonaitis, K. Olszyna and J. Meagher, *Geophys. Res. Lett.*, 1991, **18**, 9–12.
56 J. T. Herron and R. E. Huie, *J. Am. Chem. Soc.*, 1977, **99**, 5430–5435.
57 F. Su, J. G. Calvert and J. H. Shaw, *J. Phys. Chem.*, 1980, **84**, 239–246.
58 S. Saunders, M. Jenkin, R. Derwent and M. Pilling, *Atmos. Chem. Phys.*, 2003, **3**, 161–180.
59 I. Bey, D. J. Jacob, R. M. Yantosca, J. A. Logan, B. D. Field, A. M. Fiore, Q. Li, H. Y. Liu, L. J. Mickley and M. G. Schultz, *J. Geophys. Res.*, 2001, **106**, 23073–23095.
60 J. C. Rivera-Rios, T. B. Nguyen, J. D. Crounse, W. Jud, J. M. St. Clair, T. Mikoviny, J. B. Gilman, B. M. Lerner, J. B. Kaiser, J. de Gouw, A. Wisthaler, A. Hansel, P. O. Wennberg, J. H. Seinfeld and F. N. Keutsch, *Geophys. Res. Lett.*, 2014, **41**, 8645–8651.
61 D. Zhang, W. Lei and R. Zhang, *Chem. Phys. Lett.*, 2002, **358**, 171–179.
62 K. T. Kuwata and L. C. Valin, *Chem. Phys. Lett.*, 2008, **451**, 186–191.
63 T. L. Nguyen, J. Peeters and L. Vereecken, *Phys. Chem. Chem. Phys.*, 2009, **11**, 5643–5656.

64 T. L. Nguyen, R. Winterhalter, G. Moortgat, B. Kanawati, J. Peeters and L. Vereecken, *Phys. Chem. Chem. Phys.*, 2009, **11**, 4173–4183.
65 O. Horie, P. Neeb and G. K. Moortgat, *Int. J. Chem. Kinet.*, 1994, **26**, 1075–1094.
66 J. J. Orlando, G. S. Tyndall and S. E. Paulson, *Geophys. Res. Lett.*, 1999, **26**, 2191–2194.
67 E. Praske, J. D. Crounse, K. H. Bates, T. Kurtén, H. G. Kjaergaard and P. O. Wennberg, *J. Phys. Chem. A*, 2015, **119**, 4562–4572.
68 L. A. Hull, *J. Org. Chem.*, 1978, **43**, 2780–2785.
69 C. A. Taatjes, O. Welz, A. J. Eskola, J. D. Savee, A. M. Scheer, D. E. Shallcross, B. Rotavera, E. P. Lee, J. M. Dyke and D. K. Mok, *Science*, 2013, **340**, 177–180.
70 J. M. Anglada, J. M. Bofill, S. Olivella and A. Solé, *J. Am. Chem. Soc.*, 1996, **118**, 4636–4647.
71 L. Sheps, A. M. Scully and K. Au, *Phys. Chem. Chem. Phys.*, 2014, **16**, 26701–26706.
72 L. Vereecken and J. S. Francisco, *Chem. Soc. Rev.*, 2012, **41**, 6259–6293.
73 D. Cremer, E. Kraka and P. G. Szalay, *Chem. Phys. Lett.*, 1998, **292**, 97–109.
74 S. Madronich, R. B. Chatfield, J. G. Calvert, G. K. Moortgat, B. Veyret and R. Lesclaux, *Geophys. Res. Lett.*, 1990, **17**, 2361–2364.
75 A. S. Hasson, G. S. Tyndall and J. J. Orlando, *J. Phys. Chem. A*, 2004, **108**, 5979–5989.
76 M. A. Crawford, T. J. Wallington, J. J. Szente, M. M. Maricq and J. S. Francisco, *J. Phys. Chem. A*, 1999, **103**, 365–378.
77 O. Horie and G. K. Moortgat, *J. Chem. Soc., Faraday Trans.*, 1992, **88**, 3305–3312.
78 S. Gäb, W. V. Turner, S. Wolff, K. H. Becker, L. Ruppert and K. J. Brockmann, *Atmos. Environ.*, 1995, **29**, 2401–2407.
79 G. K. Moortgat, R. A. Cox, G. Schuster, J. P. Burrows and G. S. Tyndall, *J. Chem. Soc., Faraday Trans. 2*, 1989, **85**, 809–829.
80 A. Tomas, E. Villenave and R. Lesclaux, *J. Phys. Chem. A*, 2001, **105**, 3505–3514.
81 V. D. Knyazev and I. R. Slagle, *J. Phys. Chem.*, 1995, **99**, 2247–2249.
82 J. C. Owicki, L. L. Shipman and H. A. Scheraga, *J. Phys. Chem.*, 1975, **79**, 1794–1811.
83 O. Welz, J. D. Savee, D. L. Osborn, S. S. Vasu, C. J. Percival, D. E. Shallcross and C. A. Taatjes, *Science*, 2012, **335**, 204–207.
84 T. R. Lewis, M. A. Blitz, D. E. Heard and P. W. Seakins, *Phys. Chem. Chem. Phys.*, 2015, **17**, 4859–4863.
85 K. E. Leather, M. R. McGillen, M. C. Cooke, S. R. Utembe, A. T. Archibald, M. E. Jenkin, R. G. Derwent, D. E. Shallcross and C. J. Percival, *Atmos. Chem. Phys.*, 2012, **12**, 469–479.
86 D. R. Glowacki, J. Lockhart, M. A. Blitz, S. J. Klippenstein, M. J. Pilling, S. H. Robertson and P. W. Seakins, *Science*, 2012, **337**, 1066–1069.
87 J. Mao, X. Ren, L. Zhang, D. M. Van Duin, R. C. Cohen, J. H. Park, A. H. Goldstein, F. Paulot, M. R. Beaver, J. D. Crounse, P. O. Wennberg, J. P. DiGangi, S. B. Henry, F. N. Keutsch, C. Park, G. W. Schade, G. M. Wolfe, J. A. Thornton and W. H. Brune, *Atmos. Chem. Phys.*, 2012, **12**, 8009–8020.
88 W.-m. Wei, R.-h. Zheng, Y.-l. Pan, Y.-k. Wu, F. Yang and S. Hong, *J. Phys. Chem. A*, 2014, **118**, 1644–1650.
89 Y.-T. Su, H.-Y. Lin, R. Putikam, H. Matsui, M. C. Lin and Y.-P. Lee, *Nat. Chem.*, 2014, **6**, 477–483.
90 R. L. Mauldin, T. Berndt, M. Sipila, P. Paasonen, T. Petaja, S. Kim, T. Kurten, F. Stratmann, V. M. Kerminen and M. Kulmala, *Nature*, 2012, **488**, 193–196.
91 J. T. Herron, R. I. Martinez and R. E. Huie, *Int. J. Chem. Kinet.*, 1982, **14**, 201–224.
92 R. Atkinson and A. C. Lloyd, *J. Phys. Chem. Ref. Data*, 1984, **13**, 315–444.
93 D. Stone, M. Blitz, L. Daubney, N. U. Howes and P. Seakins, *Phys. Chem. Chem. Phys.*, 2014, **16**, 1139–1149.
94 T. Kurten, J. R. Lane, S. Jørgensen and H. G. Kjaergaard, *J. Phys. Chem. A*, 2011, **115**, 8669–8681.
95 C. A. Taatjes, G. Meloni, T. M. Selby, A. J. Trevitt, D. L. Osborn, C. J. Percival and D. E. Shallcross, *J. Am. Chem. Soc.*, 2008, **130**, 11883–11885.
96 J. H. Lee, D. F. Leahy, I. N. Tang and L. Newman, *J. Geophys. Res.*, 1993, **98**, 2911–2915.
97 V. G. Khamaganov and R. A. Hites, *J. Phys. Chem. A*, 2001, **105**, 815–822.
98 R. Atkinson and S. M. Aschmann, *Environ. Sci. Technol.*, 1993, **27**, 1357–1363.
99 A. A. Chew and R. Atkinson, *J. Geophys. Res.*, 1996, **101**, 28649–28653.
100 S. E. Paulson, M. Chung, A. D. Sen and G. Orzechowska, *J. Geophys. Res.*, 1998, **103**, 25533–25539.
101 A. R. Rickard, D. Johnson, C. D. McGill and G. Marston, *J. Phys. Chem. A*, 1999, **103**, 7656–7664.
102 M. Siese, K. H. Becker, K. J. Brockmann, H. Geiger, A. Hofzumahaus, F. Holland, D. Mihelcic and K. Wirtz, *Environ. Sci. Technol.*, 2001, **35**, 4660–4667.
103 M. Ehn, J. A. Thornton, E. Kleist, M. Sipila, H. Junninen, I. Pullinen, M. Springer, F. Rubach, R. Tillmann, B. Lee, F. Lopez-Hilfiker, S. Andres, I.-H. Acir, M. Rissanen, T. Jokinen, S. Schobesberger, J. Kangasluoma, J. Kontkanen, T. Nieminen, T. Kurten, L. B. Nielsen, S. Jorgensen, H. G. Kjaergaard, M. Canagaratna, M. D. Maso, T. Berndt, T. Petaja, A. Wahner, V.-M. Kerminen, M. Kulmala, D. R. Worsnop, J. Wildt and T. F. Mentel, *Nature*, 2014, **506**, 476–479.
104 T. Jokinen, M. Sipilä, S. Richters, V. M. Kerminen, P. Paasonen, F. Stratmann, D. Worsnop, M. Kulmala, M. Ehn and H. Herrmann, *Angew. Chem., Int. Ed.*, 2014, **53**, 14596–14600.
105 J. D. Crounse, H. C. Knap, K. B. Ørnsø, S. Jørgensen, F. Paulot, H. G. Kjaergaard and P. O. Wennberg, *J. Phys. Chem. A*, 2012, **116**, 5756–5762.
106 A. Kiendler-Scharr, J. Wildt, M. Dal Maso, T. Hohaus, E. Kleist, T. F. Mentel, R. Tillmann, R. Uerlings, U. Schurr and A. Wahner, *Nature*, 2009, **461**, 381–384.
107 J. Mäkelä, P. Aalto, V. Jokinen, T. Pohja, A. Nissinen, S. Palmroth, T. Markkanen, K. Seitsonen, H. Lihavainen and M. Kulmala, *Geophys. Res. Lett.*, 1997, **24**, 1219–1222.

